

MIT Open Access Articles

Editors' Choice—Coating-Dependent Electrode-Electrolyte Interface for Ni-Rich Positive Electrodes in Li-Ion Batteries

The MIT Faculty has made this article openly available. **Please share** how this access benefits you. Your story matters.

Citation: Karayaylali, Pinar et al. "Editors' Choice—Coating-Dependent Electrode-Electrolyte Interface for Ni-Rich Positive Electrodes in Li-Ion Batteries." *Journal of The Electrochemical Society* 166, 6 (March 2019): A1022 © 2019 The Author(s)

As Published: <http://dx.doi.org/10.1149/2.0461906jes>

Publisher: Electrochemical Society/IOP Publishing

Persistent URL: <https://hdl.handle.net/1721.1/130086>

Version: Final published version: final published article, as it appeared in a journal, conference proceedings, or other formally published context

Terms of use: Creative Commons Attribution-NonCommercial-NoDerivs License



OPEN ACCESS

Editors' Choice—Coating-Dependent Electrode-Electrolyte Interface for Ni-Rich Positive Electrodes in Li-Ion Batteries

To cite this article: Pinar Karayaylali *et al* 2019 *J. Electrochem. Soc.* **166** A1022

View the [article online](#) for updates and enhancements.



Coating-Dependent Electrode-Electrolyte Interface for Ni-Rich Positive Electrodes in Li-Ion Batteries

Pinar Karayaylali,^{1,z} Ryoichi Tataru,^{2,*} Yirui Zhang,¹ Kuei-Lin Chan,³ Yang Yu,⁴ Livia Giordano,^{2,4,*} Filippo Maglia,⁵ Roland Jung,⁵ Isaac Lund,⁶ and Yang Shao-Horn^{1,2,4,*,z}

¹Department of Mechanical Engineering, MIT, Cambridge, Massachusetts 02139, USA

²Research Laboratory of Electronics, MIT, Cambridge, Massachusetts 02139, USA

³Department of Materials Science and Engineering, National Tsing Hua University, Hsinchu 30013, Taiwan

⁴Department of Materials Science and Engineering, MIT, Cambridge, Massachusetts 02139, USA

⁵BMW Group, 80788 Munich, Germany

⁶BMW Group Technology Office USA, Mountain View, California 94043, USA

Surface chemistry modification of positive electrodes has been used widely to decrease capacity loss during Li-ion battery cycling. Recent work shows that coupled LiPF₆ decomposition and carbonate dehydrogenation is enhanced by increased metal-oxygen covalency associated with increasing Ni and/or lithium de-intercalation in metal oxide electrode, which can be responsible for capacity fading of Ni-rich oxide electrodes. Here we examined the reactivity of lithium nickel, manganese, cobalt oxide (LiNi_{0.6}Mn_{0.2}Co_{0.2}O₂, NMC622) modified by coating of Al₂O₃, Nb₂O₅ and TiO₂ with a 1 M LiPF₆ carbonate-based electrolyte. Cycling measurements revealed that Al₂O₃-coated NMC622 showed the least capacity loss during cycling to 4.6 V_{Li} compared to Nb₂O₅-, TiO₂-coated and uncoated NMC622, which was in agreement with smallest electrode impedance growth during cycling from electrochemical impedance spectroscopy (EIS). Ex-situ infrared spectroscopy of charged Nb₂O₅- and TiO₂-coated NMC622 pellets (without carbon nor binder) revealed blue peak shifts of 10 cm⁻¹, indicative of dehydrogenation of ethylene carbonate (EC), but not for Al₂O₃-coated NMC622. X-ray Photoelectron Spectroscopy (XPS) of charged TiO₂-coated NMC622 electrodes (carbon-free and binder-free) showed greater salt decomposition with the formation of lithium-nickel-titanium oxyfluoride species, which was in agreement with ex-situ infrared spectroscopy showing greater blue shifts of P-F peaks with increased charged voltages, indicative of species with less F-coordination than salt PF₆⁻ anion on the electrode surface. Greater salt decomposition was coupled with the increasing dehydrogenation of EC with higher coating content on the surface. This work shows that Al₂O₃ coating on NMC622 is the most effective in reducing carbonate dehydrogenation and accompanied salt decomposition and rendering minimum capacity loss relative to TiO₂ and Nb₂O₅ coating.

© The Author(s) 2019. Published by ECS. This is an open access article distributed under the terms of the Creative Commons Attribution Non-Commercial No Derivatives 4.0 License (CC BY-NC-ND, <http://creativecommons.org/licenses/by-nc-nd/4.0/>), which permits non-commercial reuse, distribution, and reproduction in any medium, provided the original work is not changed in any way and is properly cited. For permission for commercial reuse, please email: oa@electrochem.org. [DOI: 10.1149/2.0461906jes]



Manuscript received March 11, 2019. Published March 29, 2019.

Understanding electrode/electrolyte interface (EEI) is crucial to increase cycling performance and safety of Li-ion batteries.¹⁻⁶ Lithium nickel manganese cobalt oxides has been promising positive electrode materials due to their increased initial charge capacity as the nickel content increases.⁷⁻⁹ However, significant capacity loss⁷⁻⁹ and thermal instability^{8,10-13} are observed once the Ni content increases in NMC electrodes. This impedance growth and reduced capacity retention^{7,8,14,15} has been attributed to the solvent oxidation^{7,9,16,17} and greater salt decomposition.¹⁶

Numerous studies have shown that surface modification of Co-based and Ni-based positive electrode materials can increase capacity retention in Li-ion batteries. Different coating materials have been studied such as metal oxides (Al₂O₃,¹⁸⁻²¹ TiO₂,²²⁻²⁶ Nb₂O₅,^{27,28}), metal phosphates (AlPO₄,^{21,29-31}), and metal fluorides (AlF₃,³²). There are several schools of thoughts for the mechanism or physical origin to enhanced capacity retention associated with coated electrode materials. Coatings on the positive electrode would act as a protective layer that reduces parasitic reactions between the positive electrode and electrolyte³³ and a HF scavenger^{30,34-36} that suppresses the transition metal dissolution from positive electrolyte surface to the electrolyte. In addition, the coating on some oxides could trigger the formation of metal fluoride on the surface during cycling, which can reduce the electrode reactivity toward the electrolyte and decrease the impedance growth of the positive electrode surfaces.³⁵⁻³⁹ Moreover, coating materials can be converted to metal fluorides,^{37,40} reducing electrode surface reactivity toward the electrolyte. For example, Myung et al.³⁷ have shown that the Al₂O₃ coating layer might form aluminum fluoride/oxyfluoride using Time-of-Flight secondary ion mass

spectrometry (ToF-SIMS) on the Li(Li_{0.05}Ni_{0.4}Co_{0.15}Mn_{0.4}) electrode at 60°C after extensively cycled. Similarly, Lu et al.⁴⁰ have studied the AlPO₄-coated LiCoO₂⁴⁰⁻⁴² electrodes using X-ray photoelectron spectroscopy (XPS) and found Al-containing fluorides and/or oxyfluorides on the cycled coated electrodes.

More recently, density functional theory calculations^{43,44} have shown that the driving force for carbonate solvent dehydrogenation on oxides, yielding surface protic species, increased with greater Ni-content in NMC (NMC111, 622 and 811).¹⁶ Ex-situ infrared and Raman spectroscopy have revealed EC dehydrogenation^{16,43,44} on charged NMC surfaces, where resulted protic species on charged NMC surfaces can further react with LiPF₆ to generate less-fluorine-coordinated species.^{16,45,46} Greater salt decomposition was coupled with increasing EC dehydrogenation on charged NMC with increasing Ni or lithium de-intercalation.¹⁶ It is hypothesized that coating materials might have much lower thermodynamic tendency to dehydrogenate or dissociate carbonate solvents, which can reduce salt decomposition and capacity loss during cycling.^{30,33,47}

In this study, we investigate the electrochemical performances of uncoated, Al₂O₃-, Nb₂O₅- and TiO₂-coated NMC622 electrodes using LP57 electrolyte (1M LiPF₆ in ethylene carbonate (EC) and ethyl methyl carbonate (EMC) 3:7 wt:wt) by cycling measurements and electrochemical impedance spectroscopy (EIS). Density Functional Theory calculations reveal that the high band-gap compounds such as Al₂O₃ have a lower tendency to bind hydrogen than materials with smaller band gap such as TiO₂ and Nb₂O₅. While on semiconducting materials hydrogen adsorbs as a proton on the oxygen site and one electron is transferred to the metal states, for instance to the metal 3d states in the case of TiO₂, the large band of Al₂O₃ prevents this charge transfer resulting in unfavorable adsorption.⁴⁷ We employ Fourier-transform infrared spectroscopy (FT-IR) and X-ray photoelectron spectroscopy (XPS) to understand the reaction

*Electrochemical Society Member.

**Electrochemical Society Fellow.

^zE-mail: pinark@mit.edu; shaohorn@mit.edu

intermediates and salt and solvent decomposition on charged uncoated and coated NMC622 electrodes. Through those efforts, we have linked the electrochemical performances of uncoated and coated NMC622 electrodes to the solvent and salt decomposition on these electrodes, which will give information for rational design of stable positive electrode-electrolyte interfaces.

Experimental

Oxide synthesis and electrode preparation.—The pellet electrode was prepared through pelletizing around 48 mg of active materials using 6 mm diameter pressing die set (Across International) for 15 mins. The pellets were then sintered under oxygen flow at 750°C for 6 hours, for NMC622 electrodes. The cooling and heating rates are controlled to be 2°C/min. The pellet electrodes are then broken into pieces of around 3 mg each, then dry in vacuum under 120°C overnight before transferred into Argon-filled glovebox (<0.5 ppm of H₂O and O₂).

The carbon-free binder free electrodes were prepared by mixing active materials with N-methyl-2-pyrrolidone (NMP) (Sigma Aldrich) in a 1:100 mass ratio. After bath-sonication for 30 min, the ink was deposited on $\frac{1}{2}$ inch diameter aluminum discs and dried at 100°C. Composite electrodes were prepared by mixing active material (85%), carbon black (2% Csp, Timcal, 5% KS6) and polyvinylidene fluoride (PVDF) (8%, Kynar) dispersed in NMP with homogenizer (Thinky AR-100). The slurry was then bladed onto aluminum sheet with a gap of 10 μ m. Both composite and carbon-free binder-free electrodes were punched and pressed at 6.3 T cm⁻² under a hydraulic press, to favor embedding of the powder in the aluminum disc in the case of the carbon-free, binder-free electrodes. Finally, the electrodes were completely dried at 120°C under vacuum for 24 h. Al₂O₃, TiO₂ and Nb₂O₅ coated NMC622 (LiNi_{0.6}Mn_{0.2}Co_{0.2}O₂) materials prepared by atomic layer deposition (ALD) were obtained from Forge Nano.

Electrochemistry.—Electrochemical behavior of the electrodes was confirmed by galvanostatic measurements in two-electrodes cells (Tomcell type TJ-AC) and coin cell (CR2016). For coin-cell cycling, the formation cycle was done at C/10 rate (27.5 mA/g) from upper cut-off voltage (4.2, 4.4 and 4.6 V_{Li}) to 2 V_{Li} with constant current constant voltage (CCCV) charging with a cutoff current of C/20 (13.8 mA/g) for two cycles, followed by 1 C rate cycling (275 mA/g) from upper cut-off voltage (4.2, 4.4 and 4.6 V_{Li}) to 2 V_{Li}. Cells were assembled in an argon-filled glovebox (<0.5 ppm of H₂O and O₂) and comprised a lithium metal foil as the negative electrode, separated by two pieces of polypropylene separator (2500 Celgard), impregnated with 100 μ L of LP57 (1M LiPF₆ in a 3:7 ethylene carbonate (EC): ethylmethyl carbonate (EMC)) electrolyte (BASF). After assembly, the cells rested for 6 h prior to measurement and then were charged with different end-of-charge potentials (4.1, 4.2, 4.4 and 4.6 V_{Li}) at a C/100 rate, based on the theoretical capacity calculated assuming full delithiation. The cells were maintained at end-of-charge potential for 5 h before disassembly in the glovebox. Carbon-free, binder-free electrodes were gently rinsed with 100 μ L of EMC and dried under vacuum at room temperature for 3 h. No rinsing was performed for pellet electrodes to enable probing electrolyte features.

Three-electrode cells were used to investigate Electrochemical Impedance Spectroscopy (EIS) for coated-NMC622 composite electrodes. These cells were assembled in argon-filled glovebox (<0.5 ppm of H₂O and O₂) with a Li metal foil (15 mm diameter), 2 pieces of Celgard 2325 (19 mm diameter, MTI) as the separators, Li₄Ti₅O₁₂ mesh reference electrode (18 mm diameter), 2 pieces of Celgard 2325 (19 mm diameter) again, and composite electrode (1/2 inch diameter) from bottom to top, where a mesh Li₄Ti₅O₁₂ reference electrode was placed between positive and negative electrode with two separators with 200 μ L of 1 mol/L LiPF₆ in a 3:7 wt:wt ethylene carbonate (EC): ethyl methyl carbonate (EMC) electrolyte (LP57, BASF) was used as electrolyte. The composite electrodes were charged with different end-of-charge potential at 27.5 mAh/g (C/10 rate based on theoretical capacity 275 mAh/g). After 10 minutes relax, EIS measurements

were carried out at open circuit potential with 10 mV amplitude and frequency range from $\sim 10^{-2}$ to 10^6 Hz with VMP3 (Potentiostat with frequency response analyzer, Biologic), with temperature fixed at 25°C (Espec, SU-241). Additional details of cell/experimental configuration for three-electrode EIS method can be found in our previous work.⁴⁸ The resistance values from cycling data and the EIS measurements are different, which may arise from responses from negative and positive electrodes in two-electrode cells used for cycling measurements, whereas EIS measurements were made with three-electrode cell setup to measure impedance changes of the positive electrode alone.

FT-IR spectroscopy.—The Fourier transform infrared (FT-IR) spectra of the materials were obtained on an FT-IR Tensor II (Bruker) equipped with deuterated triglycine sulfate (DTGS) detector inside an argon-filled glovebox with the H₂O and O₂ levels < 0.5 ppm. The species on active materials formed during (electro)chemical process was analyzed with the diffuse reflectance infrared Fourier transform (DRIFT) accessory (Praying Mantis, Harrick scientific products). Powder samples for DRIFT measurement were prepared by mixing active materials with KBr (>99.9% FT-IR grade, Sigma Aldrich) to give the concentration of active materials of 0.2 wt%. The DRIFT measurements were done with a 4 cm⁻¹ resolution in the 4000–400 cm⁻¹ spectral range at a scan velocity of 1.6 KHz; 256 scans were averaged. All FTIR spectra of the liquid samples were recorded using a single reflection ATR accessory (Pike Vee-Max II, Pike Technologies) with a Ge prism (Pier optics) at an incident angle of 45 degrees. The ATR measurements were performed with a 4 cm⁻¹ resolution in the 4000–400 cm⁻¹ spectral ranges at a scan velocity of 1.6 KHz; 256 scans were averaged. All spectra are shown in the absorbance units defined as $\log(I_0/I)$, where I_0 and I represent the background spectra and sample spectra, respectively. The background spectrum I_0 for DRIFT and ATR measurements were measured in the pure KBr powder and blank condition, respectively.

XPS measurements.—All carbon-free, binder-free electrodes were transferred from glovebox to XPS chamber using a transfer vessel (ULVAC-PHI, INC.). For each potential, at least two electrodes were charged for reproducibility. All the XPS spectra were collected using a PHI 5000 VersaProbe II (ULVAC-PHI, INC.) using a monochromatized Al K α source and a charge neutralizer. A pass energy of 23.5 eV was used and adventitious carbon at 285 eV (C1s spectra) was used for calibration of all XPS spectra. After subtraction of a Shirley-type background, photoemission lines were fitted using combined Gaussian-Lorentzian functions, except in the case of the Co, Ni and Mn 2p_{3/2} lines where asymmetric line shapes were used. The RSF (relative sensitivity factors) values for C 1s, O 1s, F 1s, P 2p, Li 1s, Co 2p_{3/2}, Ni 2p_{3/2} and Mn 2p_{3/2}, Al 2p, Ti 2p, Nb 3d photoemission lines were given as 0.314, 0.733, 1, 0.525, 0.028, 2.3526, 2.468, 1.792, 0.256, 1.256, and 3.71, respectively. The chemical compositions, binding energies and full width at half maximum of all spectra can be found in Tables S1–S5.

Results and Discussion

Coating-dependent capacity loss and impedance growth of Al₂O₃-, Nb₂O₅- and TiO₂-coated NMC622 electrodes.—Figure 1 shows the voltage profiles of uncoated, Al₂O₃-, Nb₂O₅- and TiO₂-coated (4 monolayers) NMC622 electrodes in the first, 50th and 100th cycles (after two formation cycles) with 4.2, 4.4 or 4.6 V_{Li} cut-off potentials. In the first cycle, the charge and discharge capacities of uncoated and coated NMC622 electrodes were comparable (Figure 1a), which increases from ~ 160 mAh/g at 4.2 V_{Li}, ~ 180 mAh/g at 4.4 V_{Li} to ~ 200 mAh/g for 4.6 V_{Li}. Upon cycling to 4.2 V_{Li}, uncoated and coated NMC622 electrodes were found to have comparable capacities (for 100 cycles examined in this study), where uncoated and coated electrodes were found to have comparable voltage polarization. With increasing upper voltage cutoff, uncoated NMC622 was found to have the highest capacity loss and greatest growth in voltage polarization upon cycling to 4.6 V_{Li} in Figure 1c in comparison with coated

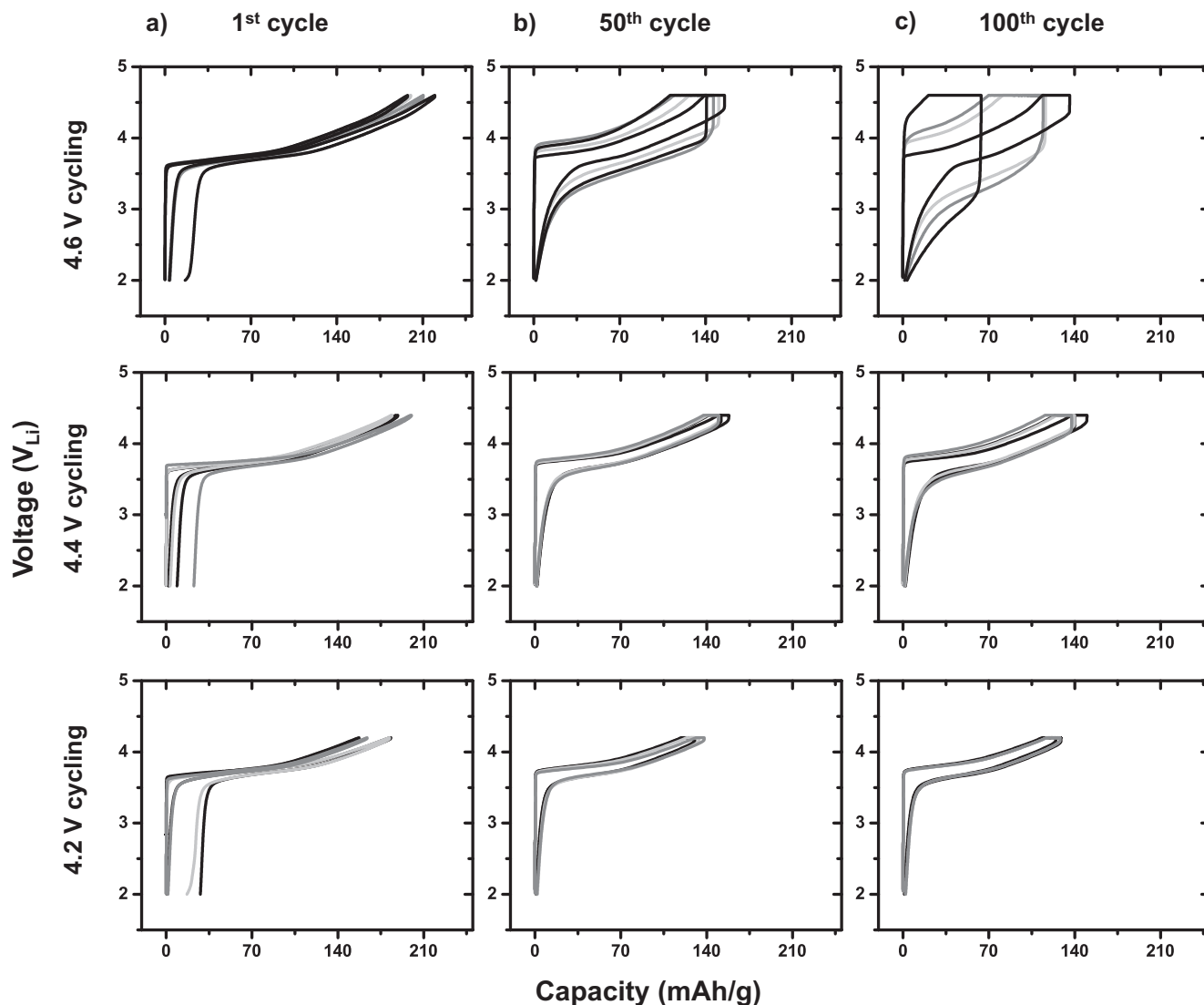


Figure 1. The capacity versus voltage for (a) 1st, (b) 50th and (c) 100th cycles for uncoated (black), Al₂O₃-coated (dark gray), Nb₂O₅-coated (light gray) and TiO₂-coated (gray) (4 monolayers) NMC622 cycled between 4.6 V_{Li}, 4.4 V_{Li}, and 4.2 V_{Li} and 2 V_{Li}. The cycle number vs capacity plots can be found in Figure S1. The charge and discharge curves were collected from two-electrode coin cells with a 1 C rate after two formation cycles (C/10 rate) in 1 M LiPF₆ in a 3:7 (w:w) EC: EMC, where C is defined as the capacity corresponding to full delithiation, and with lithium metal as the negative electrode. The resistance calculations based on electrochemical performances can be found in Figure S2.

NMC622. Among the coated electrodes, Al₂O₃-coated NMC622 electrodes had the highest capacity retention and minimum voltage polarization after 100 cycles while TiO₂-coated NMC622 electrodes had the highest capacity loss and resistance (voltage polarization).

The observed trend in the capacity loss and cell resistance growth upon cycling to 4.6 V_{Li} for uncoated and coated electrodes in Figure 1 is further supported by impedance measurements. The Nyquist plots for uncoated, Al₂O₃-, TiO₂- and Nb₂O₅-coated NMC622 composite electrodes cycled between 4.6 V_{Li} and 2 V_{Li} and EIS measurements at 4.1, 4.2 and 4.4 V_{Li} reveal two semicircles (Figure 2), where the high-frequency semicircle was assigned to the impedance associated with ion adsorption and desorption at the electrified interface while the low-frequency semicircle was attributed to the charge transfer impedance for the positive electrode.⁴⁸ This assignment is further supported by the observation that the low-frequency semicircle grew with higher charging potential from 4.1 V_{Li} to 4.4 V_{Li}, resulting from EEI layer growth and greater resistance for charge transfer, while the size of the high-frequency semicircle kept nearly constant as reported in our previous work.⁴⁸ Although R_{HF} value depends on electrolyte ionic conductivity, electronic conductivity of composite

electrode and particle size of active materials, the frequency corresponding to the high frequency (left) semicircles are consistent ($10^3 - 10^4$ Hz) with other previous works.^{48–52} In the first cycle, all electrodes had similar sizes for the high-frequency semicircle while uncoated and Al₂O₃-coated NMC622 had smaller low-frequency impedance than those found for TiO₂- and Nb₂O₅-coated NMC622. Upon cycling, the high-frequency semicircle remained unchanged while the low-frequency semicircle was found to grow, as shown in Figure 2. Of significance to note is that Al₂O₃-coated NMC622 electrodes had the lowest impedance growth for the low-frequency semicircle after 50 cycles, followed by Nb₂O₅-coated and TiO₂-coated NMC622 electrodes. This trend is consistent with that in the estimated resistance based on the cycling data collected from two-electrode cells in Figure 1.

The decreased impedance growth for the low-frequency semicircle and increased capacity retention of Al₂O₃-coated NMC622 relative to uncoated NMC622 upon cycling to 4.6 V_{Li} can be attributed to reduced (chemical) oxidation of the electrolyte on the electrode, specifically dehydrogenation of carbonate solvents to generate protic species, which can decompose electrolyte salt anion (PF₆[−]).^{16,43,53}

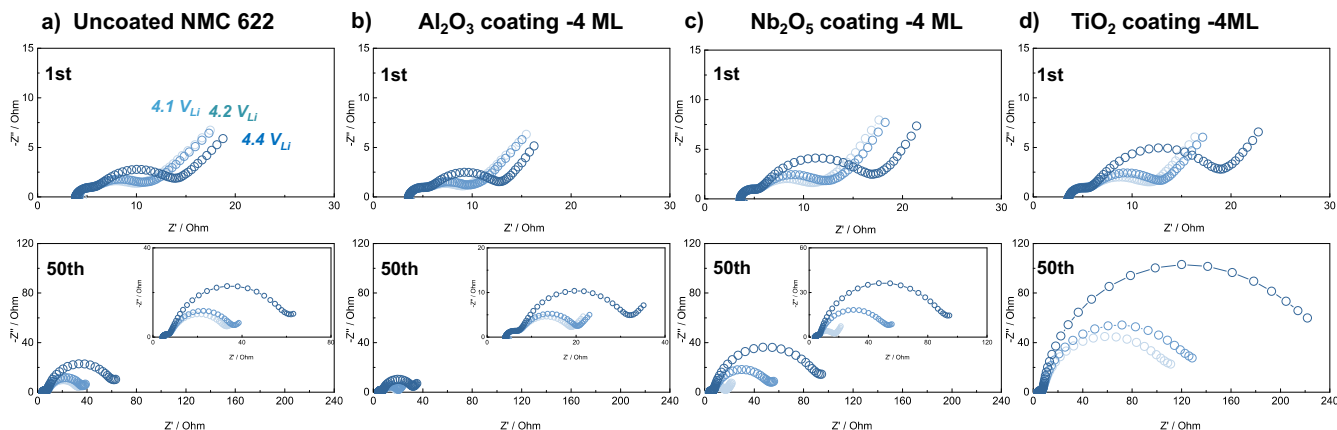


Figure 2. Nyquist plots for uncoated (a), Al_2O_3 - (b), Nb_2O_5 - (c) and TiO_2 - (d) coated NMC622 (4-monolayer) composite electrodes cycled between $4.6 V_{\text{Li}}$ and $2 V_{\text{Li}}$ with EIS collected at $4.1 V_{\text{Li}}$ (light blue), $4.2 V_{\text{Li}}$ (blue) and $4.4 V_{\text{Li}}$ (darker blue) in the first charge and after 50th cycles at 25°C . Data were collected from in three-electrode cells with mesh $\text{Li}_4\text{Ti}_5\text{O}_{12}$ reference electrode and Li metal counter electrode in 1 M LiPF_6 in a 3:7 (w:w) EC: EMC solution. The cells were galvanostatically charged at C/10 at each potential, then relax 10 minutes before EIS measurements. The electrochemical profiles for each EIS cell are shown in Figure S3 and the comparison of electrochemical performance of three-electrode EIS cell and two-electrode coin cell for cycling are shown in Figure S4.

This hypothesis is supported by much lower driving force for hydrogen adsorption on Al_2O_3 than LiMO_2 ($\text{M}=\text{Ni}, \text{Co}$) surfaces (Figure 3), which is shown to scale with the dissociation adsorption energetics of carbonate solvents in our recent work.⁵³ While TiO_2 coating has the highest tendency to dehydrogenate carbonate solvent among Al_2O_3 , Nb_2O_5 and TiO_2 coating materials (Figure 3),⁴⁷ it has lower driving force for chemical oxidation when it is compared with layered positive electrode materials such as LiCoO_2 and LiNiO_2 . This is supported by our cycling measurements of uncoated NMC 622 and TiO_2 -coated NMC622 upon cycling to $4.6 V_{\text{Li}}$, where uncoated NMC622 was found to have the higher capacity loss and the greatest growth in voltage polarization than all other coated NMC622 electrodes.

Evidence for coating-dependent dehydrogenation of carbonate solvents and salt decomposition on coated NMC622 electrodes.—DRIFT measurements of soaked and charged uncoated, Al_2O_3 , Nb_2O_5 and TiO_2 -coated NMC622 pellet electrodes (carbon-free and binder-free) revealed evidence of EC dehydrogenation, which became more pronounced when the coating changed from Al_2O_3 to TiO_2 . The DRIFT signals, originated from the stretching modes of the EC corresponding to the $\text{C}=\text{O}$ bonds, collected from charged Al_2O_3 , Nb_2O_5 and TiO_2 -coated electrodes to different end-of-charge potentials in the

first charge are compared with those of soaked electrodes (only exposure to the electrolyte) and LP57 electrolyte in Figure 4, and those of the O-C-O region are shown in Figure S6. Two distinct features at 1807 and 1773 cm^{-1} of the LP57 electrolyte¹⁶ can be assigned to the $\text{C}=\text{O}$ stretching of EC and Li^+ -coordinated EC according to our recent work,¹⁶ respectively. Below we discuss the changes from soaked electrodes to the charged uncoated and coated NMC electrodes.

No significant shift for the peaks associated with the $\text{C}=\text{O}$ stretching (centered around 1807 and 1773 cm^{-1}) was found for charged uncoated (Figure 4a) and Al_2O_3 -coated NMC622 electrodes (4-monolayer in Figure 4b and 12-monolayer in Figure 4c) relative to soaked electrodes. In contrast, these peaks were blue shifted and broadened for charged 4-monolayer TiO_2 - (Figure 4e) and Nb_2O_5 -coated (Figure 4d) NMC622, which remained largely unchanged with increasing charging voltage for 4 monolayers (Figure 4). This blue shift (that induces peak broadening) became more evident with increased coating thickness from 4 to 12 monolayers for charged TiO_2 -coated NMC622 but not for charged Al_2O_3 -coated NMC622 (Figure 4). The blue shift and peak broadening can be attributed to species derived from EC dehydrogenation formed on NMC622 electrodes as reported in our recent work,¹⁶ which is supported by the calculated spectra for the Li^+ -EC and dehydrogenated Li^+ -EC shown in Figure 4. Similar blue shifts and peak broadening were found for the O-C-O stretching of EC on charged TiO_2 -coated NMC622 while no significant shifts were noted for charged Al_2O_3 -coated NMC 622 (Figure S6). Therefore, these results revealed evidence for dehydrogenation of EC on charged TiO_2 -coated NMC622 but not Al_2O_3 -coated NMC622, which is in agreement with greater driving force for hydrogen adsorption and consequently surface dissociative adsorption of carbonate solvents on TiO_2 than Al_2O_3 from DFT results (Figure 3).⁴⁷

Comparing the P-F region of the DRIFT spectra for soaked and charged coated NMC electrodes revealed the formation of less-fluorine coordinated species, which is accompanied with carbonate dehydrogenation. Dehydrogenation of EC or EMC generates protic species such as surface hydroxyl groups,^{16,43} which can react with LiPF_6 salt to form less fluorine-coordinated species such as PF_3O or PF_5 species.^{16,46} The possible reaction mechanisms include $2^* \text{H} + \text{O}_{\text{lat}} \Rightarrow \text{H}_2\text{O} + \text{O}_{\text{vac}}$ ($^* \text{H}$ being H adsorbed at a lattice oxygen site); $\text{H}_2\text{O}_{\text{oxide}} + \text{PF}_5 \Rightarrow \text{PF}_3\text{O} + 2\text{HF}$; $\text{PF}_3\text{O} + \text{H}_2\text{O}_{\text{oxide}} \Rightarrow \text{HPF}_2\text{O}_2 + \text{HF}$; and $2\text{HF} + \text{NMC}$ and/or $\text{TiO}_2/\text{Nb}_2\text{O}_5 \Rightarrow \text{NMC-oxide/fluoride}$ and/or titanium oxyfluoride + H_2O .¹⁶ The sharp peak around 840 cm^{-1} originated from P-F stretching in LiPF_6 in the LP57 electrolyte was broadened and blue shifted for charged uncoated NMC622 with increasing charging voltage (Figure 4a), which can be attributed to the formation of less-coordinated fluorinated species at higher potentials supported by DFT simulated spectra of PF_3O and PF_6^- . In contrast, this peak was

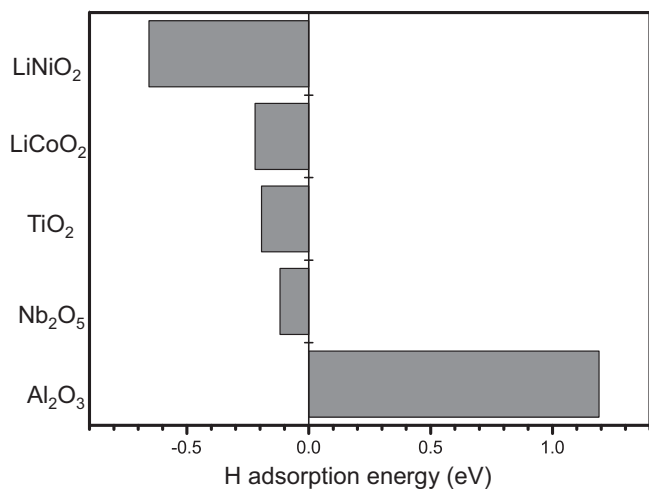


Figure 3. Hydrogen adsorption energy for positive electrode materials (LiCoO_2 and LiNiO_2) and coating materials (TiO_2 , Nb_2O_5 and Al_2O_3 compounds), computed with PBE-DFT with respect to $\frac{1}{2} \text{H}_2$ in the gas phase.⁴⁷

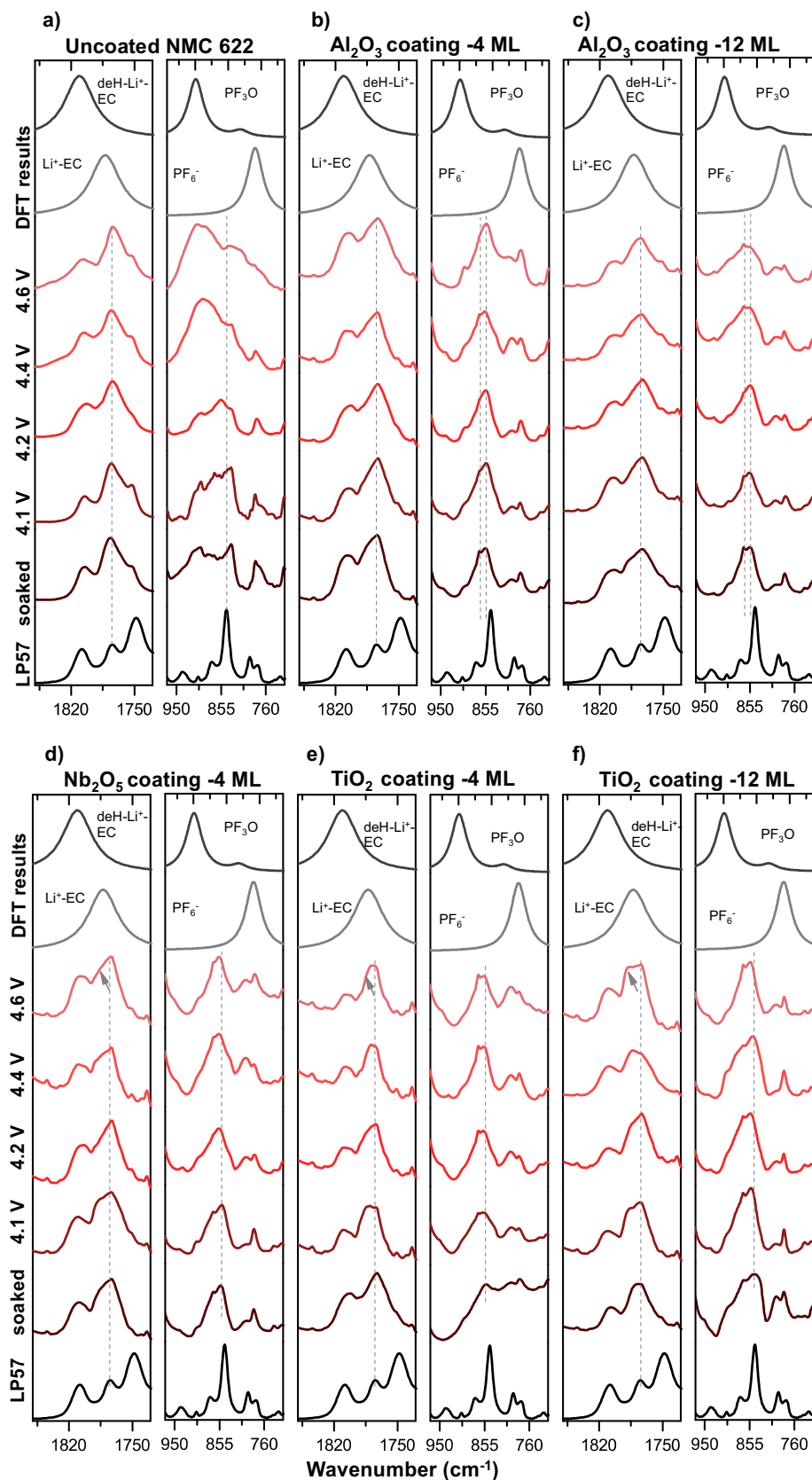


Figure 4. DRIFT spectra of C=O stretching region and P-F stretching region for (a) uncoated,¹⁶ (b) 4-monolayer Al_2O_3 -coated, (c) 12-monolayer Al_2O_3 -coated, (d) 4-monolayer Nb_2O_5 -coated, (e) 4-monolayer TiO_2 -coated and (f) 12-monolayer TiO_2 -coated NMC622 for carbon-free and binder-free pellets, in the conditions of being soaked in the LP57 electrolyte for 50 hours, and being charged to 4.1, 4.2, 4.4 or 4.6 V_{Li} . Cumulative number of 256 was used at a 4 cm^{-1} resolution. Spectra were subtracted with respect to a reference spectrum obtained with potassium bromide (KBr) powder while the ATR-IR spectrum of the pristine electrolyte is shown for comparison. The DRIFT spectra are compared with the DFT simulations of $\text{deH-Li}^+-\text{EC}$ and Li^+-EC as a reference that was previously reported by Yu et al.,¹⁶ and the peak at 1744 cm^{-1} was assigned to the C=O in EMC.¹⁶ The example electrochemistry profiles of Al_2O_3 -coated, Nb_2O_5 -coated and TiO_2 -coated NMC622 pellet electrodes are shown in Figures S5, S7-8 and the O-C-O scissoring mode for these electrodes are shown in Figures S6 and S9. The peak at 1775 cm^{-1} (shown by dashline in C=O region) and 1805 cm^{-1} was assigned to the C=O in EC and Li^+-EC respectively and the peaks around 853 cm^{-1} (shown by dashline in P-F region) are related to less-fluorine coordinated species.¹⁶

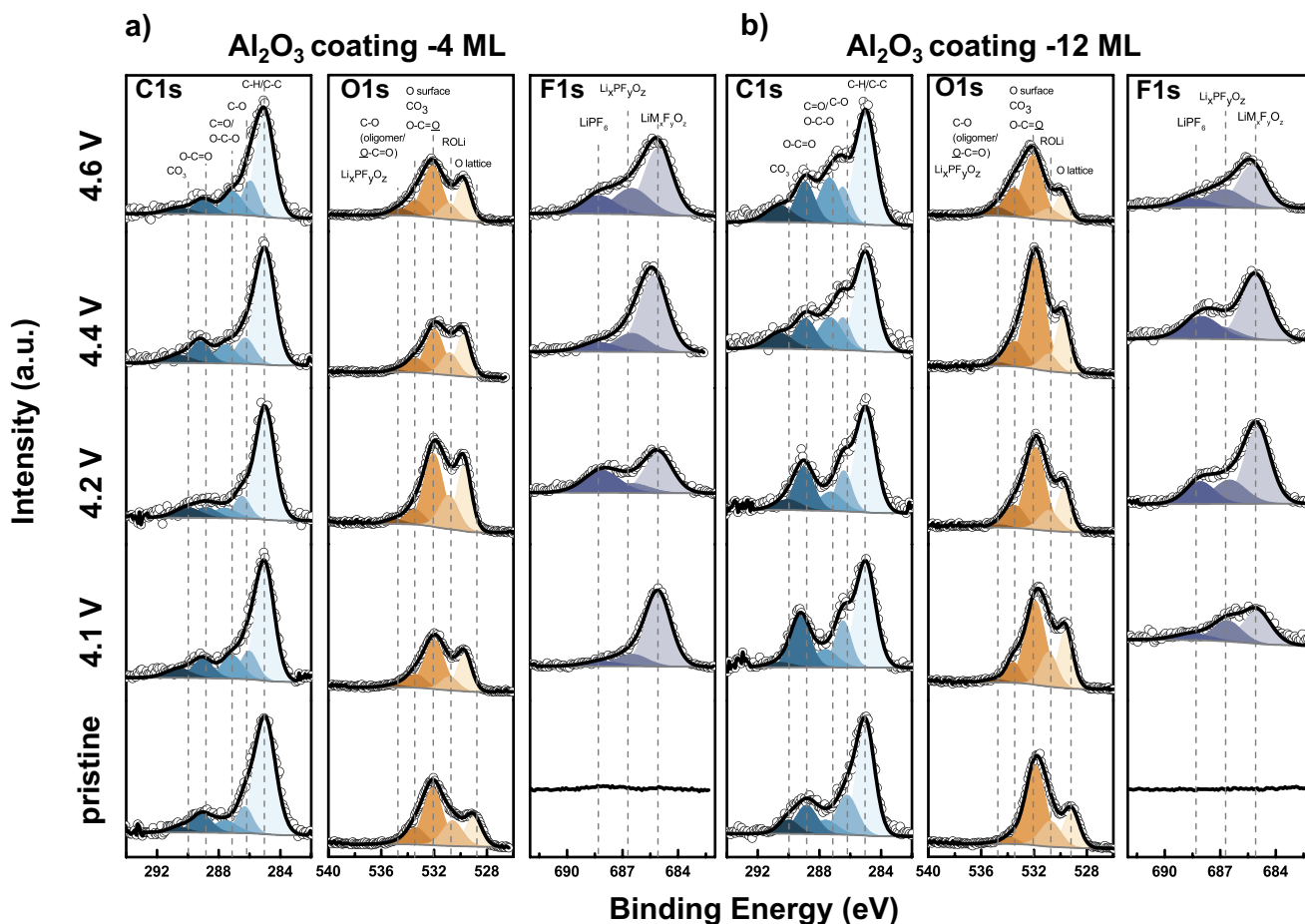


Figure 5. XPS spectra of the C 1s, O 1s and F 1s photoemission lines for Al_2O_3 -coated 4 (a) and 12 (b) monolayers for the pristine carbon-free, binder-free electrodes and after charging to 4.1, 4.2, 4.4, and 4.6 V_{Li} with 1 M LiPF_6 in EC: EMC (3:7 wt:wt) electrolyte. All spectra were calibrated with the adventitious hydrocarbons at 285.0 eV and background corrected using a Shirley background. C1s spectra were assigned with the following contributions: C-H/C-C (~ 285 eV),⁵⁴ C-O (~ 286.3 eV),⁵⁵ C=O/O-C-O (~ 287.6 eV),^{55,56} O=C-O (~ 288.8 eV)⁵⁵ and CO_3 (~ 290.3 eV).⁴¹ O1s spectra were assigned with the following contributions: O lattice (~ 529.3 eV),⁵⁷ ROLi (~ 531 eV),^{56,58} surface O/ CO_3 /O-C=O (~ 532 eV),^{41,59} C-O/O-C=O/OP(OR)₃ ($E_b \sim 533.4$ eV)^{6,56,57} and $\text{Li}_x\text{PF}_y\text{O}_z$ ($E_b \sim 534.8$ eV).⁶⁰ The F1s spectra were deconvoluted to three different species: lithium or metal fluoride species around 685 eV,⁵⁷ lithium or metal fluorophosphate around 686.5 eV⁵⁷ and lithium hexafluorophosphate around 688 eV.⁴⁶ The representative electrochemical profile is shown in Figure S10. The P 2p, Co 2p, Mn 2p, Ni 2p and Li 1s/Co 3p XPS spectra is shown in Figures S11-12, the quantification is shown in Figure S13 and Table S1-S2.

found largely unchanged for charged Al_2O_3 -coated NMC622 with increasing voltage, which is in agreement with reduced reactivity toward dehydrogenation of carbonate solvents as shown by DFT (Figure 3) and FT-IR results in comparison to charged NMC. On the other hand, the P-F stretching peak was found to be broadened considerably for charged 12-monolayer TiO_2 -coated NMC622, which was accompanied with increasing blue shift and peak broadening associated with the C=O stretching upon EC de-hydrogenation discussed earlier.

Greater reactivity toward carbonate and salt decomposition for TiO_2 -coated NMC622 than Al_2O_3 -coated NMC622 was further confirmed by XPS analysis. EEI layers formed on uncoated and Al_2O_3 -, TiO_2 - and Nb_2O_5 -coated NMC622 carbon-free, binder-free electrodes charged to different potentials were studied by XPS analysis of C 1s, O 1s, F 1s, P 2p, Mn 2p, Co 2p, Ni 2p, Li 1s, Nb 3d, Al 2p and Ti 2p spectra. The C 1s spectra were fitted to components 285.0, 286.3, 287.6 and 288.8 eV. These peaks can be attributed to adventitious carbon,⁵⁴ C-O bonds like ROLi⁵⁵ or polyethers, C=O/O-C-O bonds^{55,56} and O=C-O bonds.⁵⁵ Only small contribution for CO_3 bonds was observed around 290.3 eV.⁴¹ The growth of EEI layer supported by the O 1s spectra that revealed five contributions for charged coated samples. The lowest energy contribution at 529 eV came from O lattice from coated NMC electrodes, which could be combination of O lattice^{40,61-63} from coating or the NMC powder. The other four

peaks are attributed to ROLi (~ 531 eV),^{56,58} semicarbonates around 532 eV (ROCO_2Li and CO_3 group)^{41,59} and polyethers species around 533.4 eV (O-C=O bonds)^{6,56,57} and lithiated fluorophosphates species ($\text{Li}_x\text{PF}_y\text{O}_z$).⁶⁰ The O lattice peak is shifted to higher binding energy with increasing voltage, which is an indication of the oxyfluoride formation on the surface. These oxyfluoride species can be formed by the protic species attacking NMC622 electrode and/or coating on the surface of the electrode.¹⁶ The indicative O lattice shift to higher binding energy can be correlated with the shifts of Ni 2p, Ti 2p and Nb 3d to higher binding energy which suggests formation of lithium nickel titanium or lithium nickel niobium oxyfluorides on the surfaces of TiO_2 and Nb_2O_5 coated NMC622 electrodes (Figure 7).⁶² We still see formation of lithium nickel oxyfluorides on Al_2O_3 -coated NMC622 surfaces similar to uncoated NMC622 electrodes, however since the Al 2p spectra does not shift to higher binding energy, we do not see evidence of formation of aluminum oxyfluoride species which definitely shows less reactivity of carbonate electrolyte on Al_2O_3 -coated NMC622 than TiO_2 - and Nb_2O_5 -coated NMC622 electrodes.

Increasing tendency toward greater salt decomposition can be further confirmed by XPS analysis of their F 1s spectra in Figures 5 and 6. Figures 5 and 6 show the 4-monolayer and 12-monolayer TiO_2 - and Al_2O_3 -coated NMC622 electrodes. The intensity of F 1s spectra

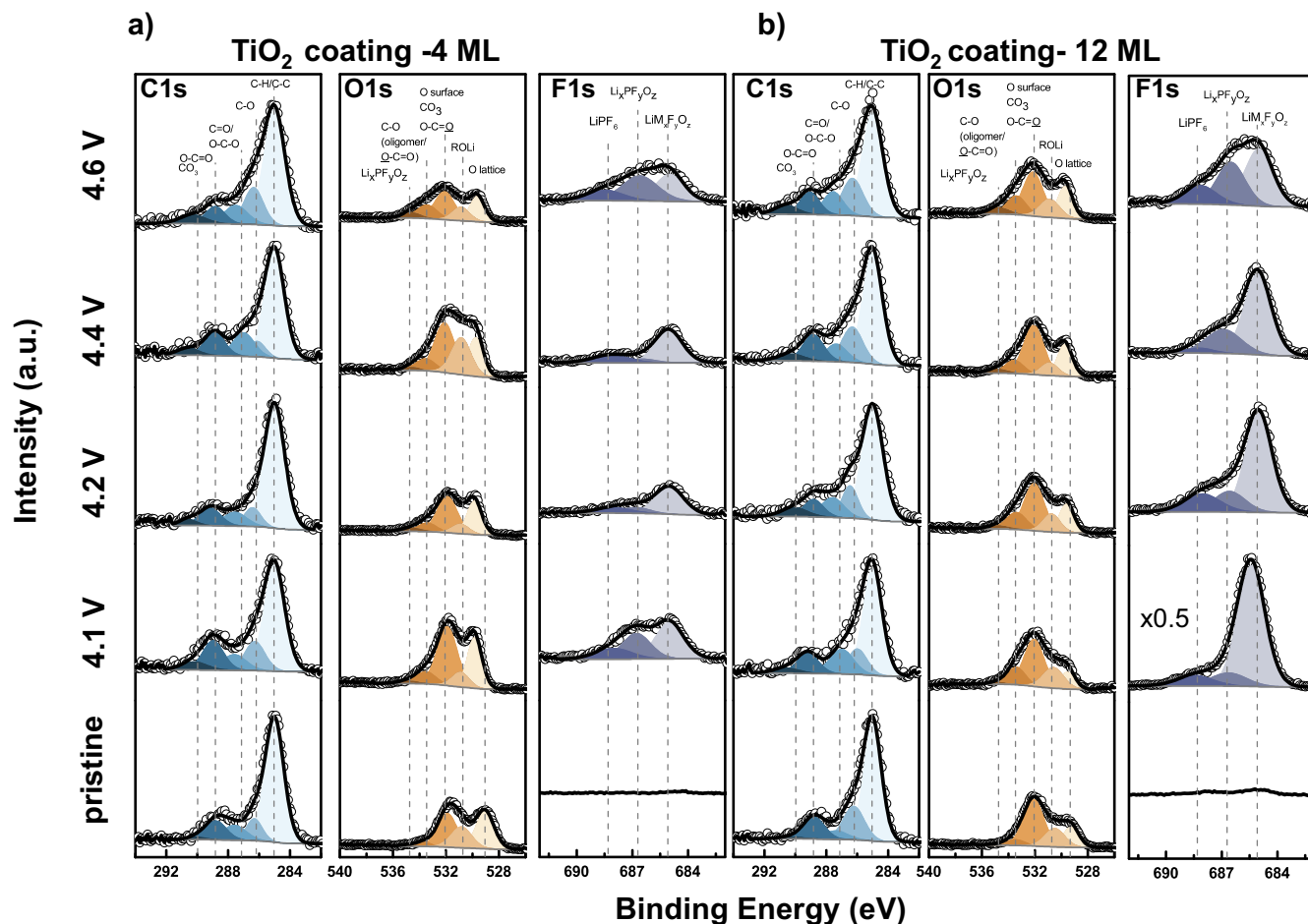


Figure 6. XPS spectra of the C 1s, O 1s and F 1s photoemission lines for TiO₂-coated 4 (a) and 12 (b) monolayers for the pristine carbon-free, binder-free electrodes and after charging to 4.1, 4.2, 4.4, and 4.6 V_{Li} with 1 M LiPF₆ in EC: EMC (3:7 wt:wt) electrolyte. All spectra were calibrated with the adventitious hydrocarbons at 285.0 eV and background corrected using a Shirley background. C1s spectra were assigned with the following contributions: C-H/C-C (~285 eV),⁵⁴ C-O (~286.3 eV),⁵⁵ C=O/O-C-O (~287.6 eV),^{55,56} O=C-O (~288.8 eV)⁵⁵ and CO₃ (~290.3 eV).⁴¹ O1s spectra were assigned with the following contributions: O lattice (~529.3 eV),⁵⁷ ROLi (~531 eV),^{56,58} surface O/CO₃/O-C=O (~532 eV),^{41,59} C-O/O-C=O/OP(OR)₃ (E_b~533.4 eV)^{6,56,57} and Li_xPF₆O₂ (E_b~534.8 eV).⁶⁰ The F1s spectra were deconvoluted to three different species: lithium or metal fluoride species around 685 eV,⁵⁷ lithium or metal fluorophosphate around 686.5 eV⁵⁷ and lithium hexafluorophosphate around 688 eV.⁴⁰ The representative electrochemical profile is shown in Figure S14. The Co 2p, Mn 2p, Ni 2p, Li 1s/ Co 3p, P 2p and Ti 2p XPS spectra is shown in Figures S15-16, the quantification is shown in Figure S17 and Table S3-S4.

is from all 4-monolayer Al₂O₃-, Nb₂O₅- and TiO₂-coated NMC622 electrodes quite similar and can be found Figures S20 and S24. As the Al₂O₃ thickness of the coating increases, the F1s spectra intensity does not change from 4-monolayer Al₂O₃ to 12-monolayer Al₂O₃ coating, which is consistent with DRIFT P-F spectra in Figure 4. However, with increasing TiO₂ coating, the F1s spectra intensity increases, especially formation of the lithium nickel titanium oxyfluoride species on the surface. The increasing F 1s intensities can be deconvoluted to lithium or other transition-metal fluorides (LiF and/or LiM_xF_yO_z) at 685.0 eV⁵⁷ and lithiated or transition metal fluorophosphates (Li_xPF₆O₂) at 686.5 eV.⁵⁷ The formation of LiM_xF_yO_z-like species can be accompanied with a higher binding energy shift at Ni 2p spectra from 854.5 eV (pristine NMC622 electrodes) to 856 eV (charged NMC622 electrodes) and Ti 2p spectra from 458.5 to 459.0 eV. These LiM_xF_yO_z-like species can be formed by the HF species attacking the coating material and/or charged NMC electrodes as suggested previously, where HF can be generated by reacting protic species from dehydrogenation of EC with LiPF₆ species.¹⁶ The intensity of the Li_xPF₆O₂-like species with respect to LiM_xF_yO_z-like species was increased considerably for charged 12-monolayer TiO₂-coated NMC622 electrodes with increasing potential, which suggests greater reactivity of LiPF₆ salt with more protic species produced from dehydrogenation of EC. Although the ratio of Li_xPF₆O₂

to LiM_xF_yO_z-like species was similar for both 4-monolayer and 12-monolayer Al₂O₃ coated NMC622 electrodes, the ratio of these species has been significantly changed when the thickness of the TiO₂ coating increased from 4-monolayer to 12-monolayer which indicates the increasing salt decomposition triggered by protic species derived from EC dehydrogenation (Figure S25).^{16,43}

There are several reports on aluminum-based coated positive electrodes showing better electrochemical performance than uncoated positive electrodes such as Al₂O₃ coated-LiCoO₂ cycled at 4.3 V_{Li}⁶⁴ and 4.4 V_{Li},⁶⁵ Al₂O₃-coated NMC111 cycled at 4.5 V_{Li},⁶⁶ Al(OH)₃ coated - Li[Li_{0.2}Ni_{0.2}Mn_{0.6}]O₂ cycled at 4.6 V_{Li}.⁶⁷ One important protection mechanism that has been discussed in previous works is called HF-scavenging^{30,34-36} where coating material reacts with HF and forms metal fluoride species on the surface (e.g. Al₂O₃ + 6HF = > 2AlF₃ + 3H₂O) and would reduce the electrolyte reactivity on positive electrode surfaces and improve voltage polarization.^{27,36} However, in this work, we showed that Al₂O₃-coated NMC622 electrodes had the minimum voltage polarization and lowest impedance growth and DRIFT C=O region and XPS F 1s analysis did not reveal obvious signs of EC dehydrogenation and formation of aluminum fluoride/oxyfluoride on Al₂O₃-coated NMC622 electrodes whereas the worst electrochemical performance was shown by TiO₂-coated NMC622, where we showed clear signs of EC dehydrogenation and greater salt decomposition

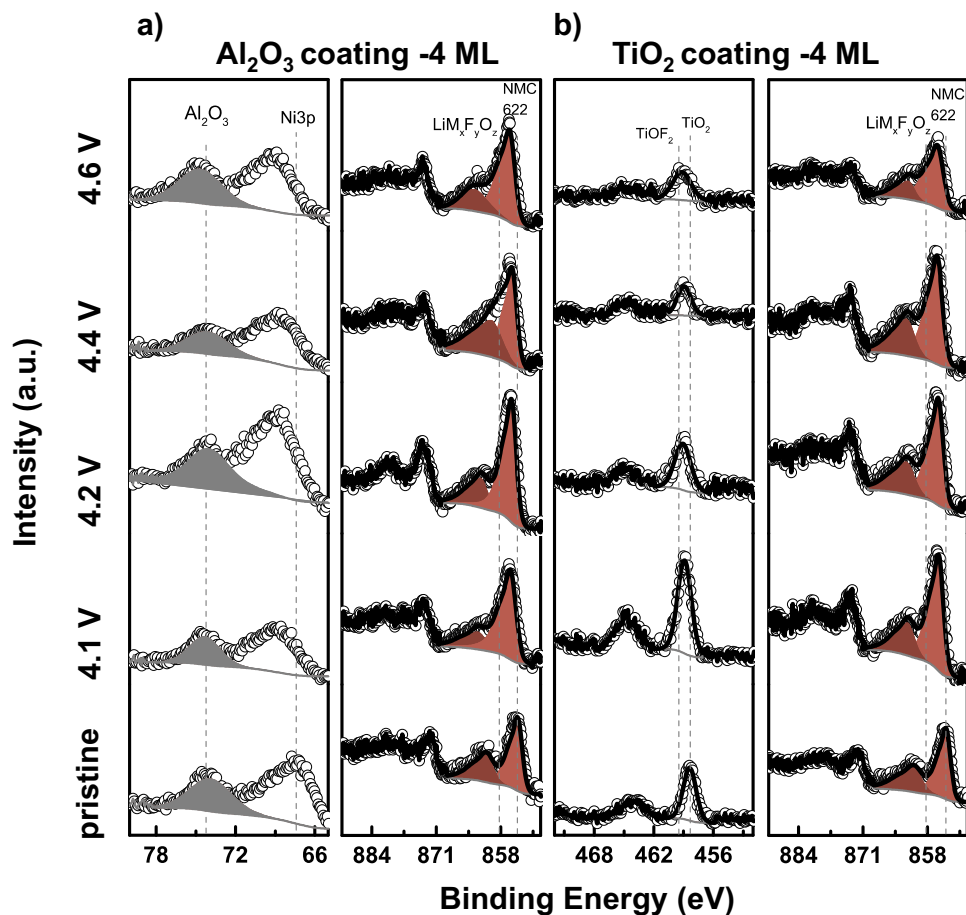


Figure 7. XPS spectra of the Ni 2p, Al 2p and Ti 2p photoemission lines for (a) Al_2O_3 -coated (4 monolayers) and (b) TiO_2 -coated (4 monolayers) for pristine and charged carbon-free, binder-free electrodes to 4.1, 4.2, 4.4, and 4.6 V_{Li} with 1 M LiPF_6 in EC: EMC (3:7 wt:wt) electrolyte. All spectra were calibrated with the adventitious hydrocarbons at 285.0 eV and background corrected using a Shirley background. The representative electrochemical profile is shown in Figure S18. The Co 2p, Mn 2p, Ni 2p and Li 1s/Co 3p XPS spectra is shown in Figures S19-23, the quantification is shown in Figure S24 and Table S1 and S3.

including formation of lithium-nickel-titanium oxyfluoride species. Dahn et al.²⁶ reported the titanium-based coated on NMC532 electrodes can help preventing transition metal dissolution and improve the cycling performance. This may be the reason why we have also seen better electrochemical performance for TiO_2 -coated NMC622 than uncoated NMC622 using two-electrode coin cell setup. However, our three-electrode EIS cell measurements indicate TiO_2 -coated NMC622 has higher impedance growth than uncoated NMC622, since we only observe the effect of positive electrode side, mainly the effect of EC dehydrogenation. These results can be further supported by our recent work,⁴⁷ where we show Al_2O_3 has lower tendency to bind hydrogen than TiO_2 and Nb_2O_5 coating materials, so as we lower the Fermi level with respect to O-p band (from Al_2O_3 to TiO_2), the dissociation of EC molecule where protic species such as surface hydroxyl groups are formed becomes more thermodynamically favorable. We propose that the high band-gap insulators such as Al_2O_3 are the best coating materials due to their lower reactivity with electrolyte solvents and salts.

Conclusions

This work combines EIS, DRIFT and XPS spectroscopies together with cycling measurement to understand the reactivity of coating materials on NMC622 electrodes toward carbonate electrolyte with LiPF_6 salt and this reactivity is linked with the impedance and cycling measurements. By combining cycling and EIS measurements, we show

coating-dependent electrochemical performance of NMC622 upon cycling to 4.6 V_{Li} . Al_2O_3 -coated NMC622 had reduced capacity loss and impedance growth while TiO_2 -coated NMC622 had greater capacity loss and impedance growth than uncoated NMC622. Combining XPS and DRIFT measurements on C=O and P-F regions, we show evidence for dehydrogenation of EC on TiO_2 -coated NMC622 positive electrodes, where it forms protic species and these protic species can react with LiPF_6 salt to form less-fluorine coordinated species such as PF_3O -like (DRIFT) and lithium nickel titanium or niobium oxyfluoride species (XPS). Exposing NMC622 surface more to TiO_2 coating makes the surface more prone to dehydrogenation of EC and formation of less-fluorine coordinated species. Through these key findings, we propose key reaction intermediates for TiO_2 and Al_2O_3 coating on NMC622 and we believe Al_2O_3 coating should be used for Ni-rich positive electrodes such as NMC622 due to reduced reactivity toward chemical oxidation of carbonate solvents and the development of stable positive electrode-electrolyte interface during cycling.

Acknowledgment

This work made use of the MRSEC Shared Experimental Facilities at MIT, supported by the National Science Foundation under award number DMR-1419807. Research at MIT related to this work was supported financially by BMW.

ORCID

Ryoichi Tatara  <https://orcid.org/0000-0002-8148-5294>Yang Shao-Horn  <https://orcid.org/0000-0001-8714-2121>

References

1. S. Menkin, D. Golodnitsky, and E. Peled, *Electrochem. Commun.*, **11**, 1789 (2009).
2. A. Smith, J. Burns, S. Trussler, and J. Dahn, *J. Electrochem. Soc.*, **157**, A196 (2010).
3. M. Gauthier et al., *J. Phys. Chem. Lett.*, **6**, 4653 (2015).
4. K. Xu, *Chem. Rev.*, **114**, 11503 (2014).
5. M. Winter, *Z. Für Phys. Chem.*, **223**, 1395 (2009).
6. K. Edström et al., *Electrochimica Acta*, **50**(2–3), 397 (2004).
7. R. Jung, M. Metzger, F. Maglia, C. Stinner, and H. A. Gasteiger, *J. Electrochem. Soc.*, **164**, A1361 (2017).
8. H.-J. Noh, S. Youn, C. S. Yoon, and Y.-K. Sun, *J. Power Sources*, **233**, 121 (2013).
9. S. Hwang et al., *APL Mater.*, **4**, 096105 (2016).
10. Y.-K. Sun et al., *Nat. Mater.*, **8**, 320 (2009).
11. S. Hwang et al., *Chem. Mater.*, **27**, 3927 (2015).
12. S.-M. Bak et al., *ACS Appl. Mater. Interfaces*, **6**, 22594 (2014).
13. N. Zhang et al., *Chem. Mater.*, **30**, 8852 (2018).
14. W. Liu et al., *Angew. Chem. Int. Ed.*, **54**, 4440 (2015).
15. F. Schipper et al., *J. Electrochem. Soc.*, **164**, A6220 (2017).
16. Y. Yu et al., *J. Phys. Chem. C*, **122**, 27368 (2018).
17. R. Jung et al., *J. Electrochem. Soc.*, **165**, A132 (2018).
18. B. Han et al., *ACS Appl. Mater. Interfaces*, **9**, 14769 (2017).
19. B. Han et al., *ACS Appl. Mater. Interfaces*, **9**, 41291 (2017).
20. A. M. Wise et al., *Chem. Mater.*, **27**, 6146 (2015).
21. J. Cho et al., *J. Power Sources*, **146**, 58 (2005).
22. G. T.-K. Fey, C.-Z. Lu, J.-D. Huang, T. P. Kumar, and Y.-C. Chang, *J. Power Sources*, **146**, 65 (2005).
23. H.-M. Cheng et al., *J. Phys. Chem. C*, **116**, 7629 (2012).
24. X. Zhang et al., *Adv. Energy Mater.*, **3**, 1299 (2013).
25. S.-J. Kim et al., *J. Power Sources*, **304**, 119 (2016).
26. L. Ma et al., *ACS Appl. Energy Mater.*, **1**, 7052 (2018).
27. S.-T. Myung et al., *J. Phys. Chem. C*, **111**, 4061 (2007).
28. R. Muruganantham, M. Sivakumar, and R. Subadevi, *Ionics*, **24**, 989 (2018).
29. J. Cho, Y. Kim, B. Kim, J. Lee, and B. Park, *Angew. Chem. Int. Ed.*, **42**, 1618 (2003).
30. M. Aykol et al., *Nat. Commun.*, **7**, 13779 (2016).
31. J.-G. Lee, B. Kim, J. Cho, Y.-W. Kim, and B. Park, *J. Electrochem. Soc.*, **151**, A801 (2004).
32. Y.-K. Sun, S.-W. Cho, S.-T. Myung, K. Amine, and J. Prakash, *Electrochimica Acta*, **53**, 1013 (2007).
33. Z. Chen, Y. Qin, K. Amine, and Y.-K. Sun, *J. Mater. Chem.*, **20**, 7606 (2010).
34. N. Van Landschoot, E. M. Kelder, P. J. Kooyman, C. Kwakernaak, and J. Schoonman, *J. Power Sources*, **138**, 262 (2004).
35. Y.-K. Sun, Y.-S. Lee, M. Yoshio, and K. Amine, *Electrochem. Solid-State Lett.*, **5**, A99 (2002).
36. M. Aykol, S. Kirklin, and C. Wolverton, *Adv. Energy Mater.*, **4**, 1400690 (2014).
37. S.-T. Myung et al., *Chem. Mater.*, **17**, 3695 (2005).
38. S.-T. Myung, K. Amine, and Y.-K. Sun, *J. Mater. Chem.*, **20**, 7074 (2010).
39. S.-T. Myung et al., *ACS Energy Lett.*, **2**, 196 (2016).
40. Y.-C. Lu, A. N. Mansour, N. Yabuuchi, and Y. Shao-Horn, *Chem. Mater.*, **21**, 4408 (2009).
41. A. T. Appapillai, A. N. Mansour, J. Cho, and Y. Shao-Horn, *Chem. Mater.*, **19**, 5748 (2007).
42. R. A. Quinlan, Y.-C. Lu, D. Kwabi, Y. Shao-Horn, and A. N. Mansour, *J. Electrochem. Soc.*, **163**, A300 (2016).
43. L. Giordano et al., *J. Phys. Chem. Lett.*, **8**, 3881 (2017).
44. K. Leung, *J. Phys. Chem. C*, **116**, 9852 (2012).
45. A. Guéguen et al., *J. Electrochem. Soc.*, **163**, A1095 (2016).
46. L. Terborg et al., *Anal. Chim. Acta*, **714**, 121 (2012).
47. L. Giordano et al., *submitted*.
48. R. Tatara et al., *J. Electrochem. Soc.*, **166**, A5090 (2019).
49. H. Zheng, H. Zhang, Y. Fu, T. Abe, and Z. Ogumi, *J. Phys. Chem. B*, **109**, 13676 (2005).
50. M. Thomas, P. G. Bruce, and J. B. Goodenough, *J. Electrochem. Soc.*, **132**, 1521 (1985).
51. D. Aurbach et al., *J. Electrochem. Soc.*, **145**, 3024 (1998).
52. H. Nara et al., *Electrochimica Acta*, **241**, 323 (2017).
53. T. M. Østergaard et al., *J. Phys. Chem. C* (2018).
54. J. Matthew, *Surf. Interface Anal.*, **36**, 1647 (2004).
55. H. Ago et al., *J. Phys. Chem. B*, **103**, 8116 (1999).
56. C. Kozłowski and P. M. Sherwood, *J. Chem. Soc. Faraday Trans. 1 Phys. Chem. Condens. Phases*, **81**, 2745 (1985).
57. S. Verdier et al., *J. Electrochem. Soc.*, **154**, A1088 (2007).
58. S. Malmgren et al., *Electrochimica Acta*, **97**, 23 (2013).
59. J.-C. Dupin, D. Gonbeau, H. Benqlilou-Moudden, P. Vinatier, and A. Levasseur, *Thin Solid Films*, **384**, 23 (2001).
60. H. Bryngelsson, M. Stjerndahl, T. Gustafsson, and K. Edström, *J. Power Sources*, **174**, 970 (2007).
61. M. Gauthier et al., *J. Electrochem. Soc.*, **165**, A1377 (2018).
62. W.-H. Ryu, D.-H. Kim, S.-H. Kang, and H.-S. Kwon, *RSC Adv.*, **3**, 8527 (2013).
63. R. Genieser et al., *J. Power Sources*, **373**, 172 (2018).
64. H.-J. Kwon et al., *J. Power Sources*, **126**, 156 (2004).
65. J. Cho, Y. J. Kim, and B. Park, *Chem. Mater.*, **12**, 3788 (2000).
66. Y. Kim, H. S. Kim, and S. W. Martin, *Electrochimica Acta*, **52**, 1316 (2006).
67. Y.-J. Kang, J.-H. Kim, S.-W. Lee, and Y.-K. Sun, *Electrochimica Acta*, **50**, 4784 (2005).